In Situ Spectroscopy

International Edition: DOI: 10.1002/anie.201409482
German Edition: DOI: 10.1002/ange.201409482

Microimaging of Transient Concentration Profiles of Reactant and Product Molecules during Catalytic Conversion in Nanoporous Materials**

*Tobias Titze, Christian Chmelik, Jens Kullmann, Lutz Prager, Erich Miersemann, Roger Gläser, Dirk Enke, Jens Weitkamp, and Jörg Kärger**

Abstract: *Microimaging by IR microscopy is applied to the recording of the evolution of the concentration profiles of reactant and product molecules during catalytic reaction, notably during the hydrogenation of benzene to cyclohexane by nickel dispersed within a nanoporous glass. Being defined as the ratio between the reaction rate in the presence of and without diffusion limitation, the effectiveness factors of catalytic reactions were previously determined by deliberately varying the extent of transport limitation by changing a suitably chosen system parameter, such as the particle size and by comparison of the respective reaction rates. With the novel options of microimaging, effectiveness factors become accessible in a single measurement by simply monitoring the distribution of the reactant molecules over the catalyst particles.*

Detection and exploitation of novel synthesis pathways over the past few years[1] have given rise to an impressive wealth of novel nanoporous materials.[2,3] They offer unprecedented potential for the production of new activity- and selectivity-enhanced catalysts.[4] These endeavors include the design of catalyst particles with transport properties optimized with respect to the desired reaction.[5]

[*] T. Titze, Dr. C. Chmelik, Prof. J. Kärger
Department of Interface Physics, University of Leipzig
Linnéstrasse 5, 04103 Leipzig (Germany)
E-mail: kaerger@physik.uni-leipzig.de
J. Kullmann, Prof. R. Gläser, Prof. D. Enke
Institute of Chemical Technology, University of Leipzig
Linnéstrasse 3, 04103 Leipzig (Germany)
Dr. L. Prager
Leibniz Institute of Surface Modification
Permoserstrasse 15, 04318 Leipzig (Germany)
Prof. E. Miersemann
Department of Mathematics, University of Leipzig
Augustusplatz 10/11, 04109 Leipzig (Germany)
Prof. J. Weitkamp
Institute of Chemical Technology, University of Stuttgart
Pfaffenwaldring 55, 70569 Stuttgart (Germany)

[**] Financial support by the German Science Foundation (DFG) and Fonds der Chemischen Industrie is gratefully acknowledged. Two of us (J.K. and J.W.) express their gratitude to Lothar Riekert for having brought them together three decades ago and for having raised their interest in the interplay of diffusion and reaction in nanoporous materials.

Supporting information for this article is available on the WWW under http://dx.doi.org/10.1002/anie.201409482.

The in situ observation of molecular transport and conversion remained, however, a challenging task. Though the fundamental laws of interdependence between diffusion and reaction were formulated by Jüttner[6] more than a century ago and proved to serve, via the Thiele concept,[7] as an excellent tool for analyzing diffusion-limited reactions,[8–12] the experimental techniques available to date provided only limited insight into the intrinsic phenomena of mass transfer and conversion in nanoporous materials. This is in particular true with respect to the evolution of the intrinsic profiles of the concentration of the reactant and product molecules, which remained inaccessible by direct observation. Though PFG NMR has been successfully employed for observing the diffusion and conversion of the various molecular species involved in catalytic reactions,[13] it fails to give any insight into the interplay of diffusion and reaction.

Allowing the trajectories of the molecules involved to be followed and the position of their conversion to be localized, the recent advent of single-molecule observation[14] and microspectroscopy[15] were an important step ahead.[2,16,17] Being concerned with the behavior of individual molecular species, information about the concentrations of these species has to be attained by considering the average over many trajectories. The accuracy of the spatial and temporal derivatives of the concentrations appearing in the Thiele–Jüttner concept thus remains limited. With the option of IR microimaging[18,19] to follow the evolution of the concentration profiles of all molecules involved, this type of experiment has now become possible.

We present the application of this technique to the hydrogenation of benzene to cyclohexane by nickel dispersed within a nanoporous glass.[20] This host material was applied in diffusion studies confirming the ergodic theorem for guest diffusion in nanoporous materials[17] and the compatibility of macroscopic and microscopic diffusion measurements.[21] Benzene hydrogenation on the other hand proved to be ideally suited as a model reaction. It can proceed under experimental conditions compatible with the requirements of IR microimaging, and being intrinsically first order in benzene, offers favorable conditions for mathematical analysis.[22–24]

Figure 1 introduces the procedure. Hydrogenation is initiated by bringing a benzene–hydrogen atmosphere into contact with the initially empty catalyst. The local concentrations of benzene and cyclohexane are determined by recording the spatial dependence of the attenuation of the IR light beam passing the sample, using the frequency range of

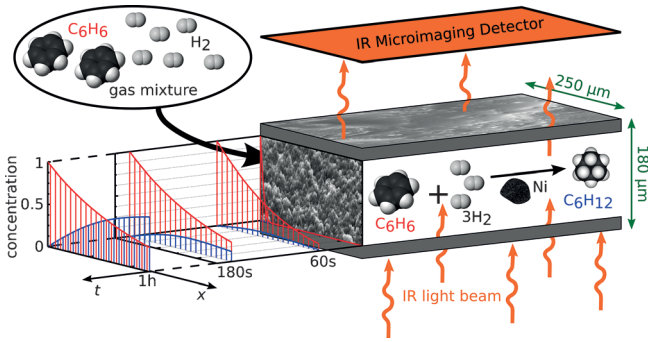

Figure 1. Monitoring reactant and product concentration profiles during the conversion of benzene (red) into cyclohexane (blue) in nanoporous materials by microimaging, with the arrows in green indicating the spatial extensions relevant for our experiments.

IR-active molecular vibrations as a fingerprint for the respective molecular species. Examples of the profile evolution for both benzene (red) and cyclohexane (blue) are shown on the left.

The nanoporous glass used as a catalyst support for the nickel nanoparticles was applied as small platelets of 180 µm thickness. Top and bottom faces were sealed gas-tight by coating with a thin silica layer (Supporting Information), allowing molecular uptake and release to take place through the edge of the platelets only. Profiles were recorded perpendicular to these edges (x direction).

Figure 2 shows the complete set of profiles recorded at 26 °C and 75 °C. Equivalent presentations for 50 °C and 100 °C are provided in the Supporting Information, Figure S7. Deficiencies close to the sample edges in both the structural homogeneity of the glass platelets and the evidence of IR imaging prohibit, in this range, a proper measurement of concentrations. The respective data points are given in gray.

Benzene is seen to propagate into the interior of the catalyst particle forming a well-shaped propagation front. This process is accompanied by the appearance of cyclohexane, emerging as a result of benzene hydrogenation. Benzene concentrations are seen to decay towards the particle interior, indicating benzene influx. Cyclohexane concentration, in contrast, decreases towards the particle boundary, indicating efflux. Both profiles approach a steady state in which the cyclohexane efflux is compensated by the benzene-to-cyclohexane conversion rate. The situation considered in the Thiele concept of correlating diffusion and reaction[8–12] does thus appear to become directly accessible. As expected, the rate of benzene propagation and the amount of cyclohexane resulting from the hydrogenation process increase with increasing temperature.

For contemplating the experimentally determined profiles within the frame of diffusion–conversion theory, we consider the relevant equation in the form:[25]

$$\frac{\partial c_A}{\partial t} = D\frac{\partial^2 c_A}{\partial x^2} - kc_A \qquad (1)$$

$$\frac{\partial c_B}{\partial t} = D\frac{\partial^2 c_B}{\partial x^2} + kc_A \qquad (2)$$

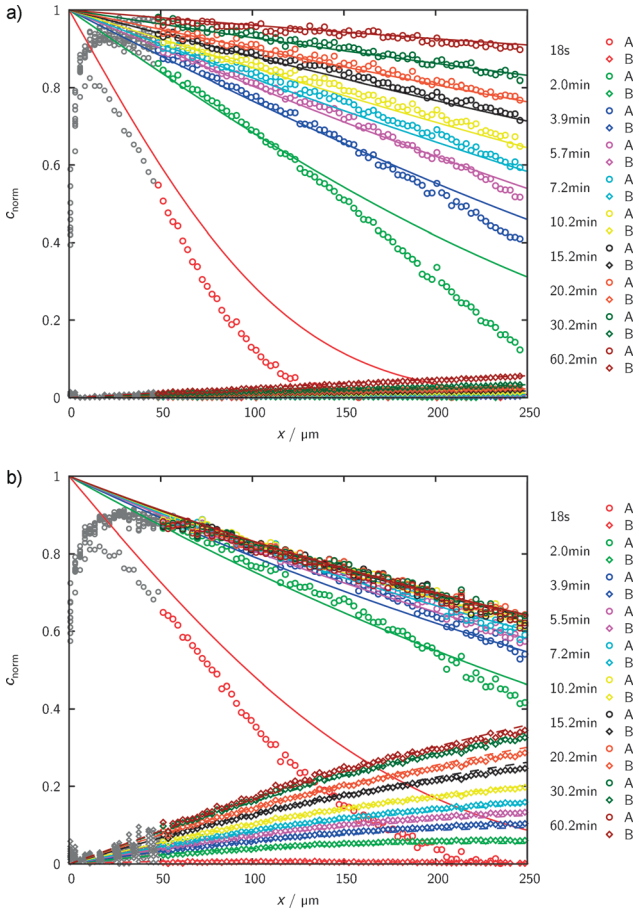

Figure 2. Transient concentration profiles during hydrogenation of benzene to cyclohexane (a: 26 °C; b: 75 °C). The experiments are started by contacting an initially empty catalyst with a benzene–hydrogen atmosphere (a: at 26 °C with $p_{benzene} = 6$ mbar; $p_{hydrogen} = 737$ mbar, b: at 75 °C with $p_{benzene} = 27$ mbar; $p_{hydrogen} = 977$ mbar). Data points represent the experimental results obtained by IR microimaging (circles: benzene (A), diamonds: cyclohexane (B)), reflecting meaningful concentrations for $x \geq 50$ µm. The solid (benzene (A)) and dashed (cyclohexane (B)) lines are results of the analytical solution [Supporting Information, Eqs. (S33),(S42)] of the diffusion–reaction equation [Eqs. (1),(2)] with the associated initial and boundary conditions [Eqs. (3),(4)]. A complete representation of the solutions (covering the whole of the distance, $0 \leq x \leq 2L = 1800$ µm, between the opposite edges of the catalyst particle) is shown in Figure 3.

with A and B referring, respectively, to benzene and cyclohexane and k denoting the first-order reaction rate constant. It is assumed that mass transfer is exclusively directed perpendicular to the edge of the platelets and that the effective diffusivities D of the two components coincide, being independent of guest concentration and composition. We skip the appendage "effective" in the following, as it is generally associated with the understanding that the diffusivity is not a genuine one and that it might be deduced from more fundamental data like bulk diffusivities and tortuosities (which is totally true with large enough pores). In fact, with pore sizes of nanometers and sample extensions of hundreds of micrometers, the concentrations appearing in Eqs. (1) and (2) can be completely meaningfully determined with reference to unit volumes with sizes notably exceeding the

individual pore size,[12,26] warranting a genuine (often referred to as "intrinsic") diffusivity as a well-defined quantity. The diffusivities in this very system are reported[21] to be determined in complete mutual agreement by a series of both microscopic and macroscopic techniques of measurement, making nanoporous glasses a model system for consistency checks of diffusion measurement with nanoporous materials. The irregular structure of the material did, on the other hand, allow for nothing more than meaningful order-of-magnitude predictions.[21]

The initial and boundary conditions

$$c_A(x,t=0) = c_B(x,t=0) = 0 \quad (3)$$

$$c_A(x=\pm L,t) = 1, \quad c_B(x=\pm L,t) = 0 \quad (4)$$

reflect the experimental situation where an initially empty catalyst [Eq. (3)] is positioned, at time $t=0$, in a benzene atmosphere which maintains, from now on, the boundary concentration of benzene at a constant value [Eq. (4)]. $L=0$ and $x=\pm L$ denote, correspondingly, positions in the platelet center and on the edges opposite each other. Figure 3 shows the complete spatial and temporal dependence as given by the analytical solution of Equations (1) and (2) [Supporting Information, Eqs. (S33),(S42)], with the diffusivity D and the reaction rate constant k resulting as the best fit to the profiles experimentally determined. All experimental profiles are, in turn, complemented with representations of the relevant parts of the solution.

Both the diffusivity and the reaction rate constant are known to be functions of also molecular concentrations.[8–12] Therefore, to ensure a meaningful comparison of the experimental results at different temperatures, the benzene pressure in the surrounding atmosphere was increased with increasing temperature so that in all cases, the equilibrium concentration of the guest molecules corresponded to about one half of total pore filling (see the Supporting Information for complete data representation). Figure 4 shows, in an Arrhenius plot, the reaction rate constants and diffusivities as resulting from the best fit between the solution of Equations (1) to (4) and the experimentally recorded profiles. The straight lines show the best fit of these data to the respective Arrhenius dependencies

$$k = k_0 \exp(-E_k/RT) \quad (5)$$

and

$$D = D_0 \exp(-E_D/RT) \quad (6)$$

with $E_D = 15.6 \pm 2.7\ \mathrm{kJ\,mol^{-1}}$ and $E_k = 48.1 \pm 4.9\ \mathrm{kJ\,mol^{-1}}$ denoting the activation energies of diffusion and reaction. With an activation energy E_D notably below the heat of adsorption of about 50 $\mathrm{kJ\,mol^{-1}}$,[27] diffusion of the reactant and product molecules may be concluded to remain essentially unaffected by desorption from surface sites as observed for example previously.[28]

The spatial and temporal dependencies of the concentration profiles are seen to be reasonably well reflected by the solution of the diffusion–reaction equations [Eqs. (1) and

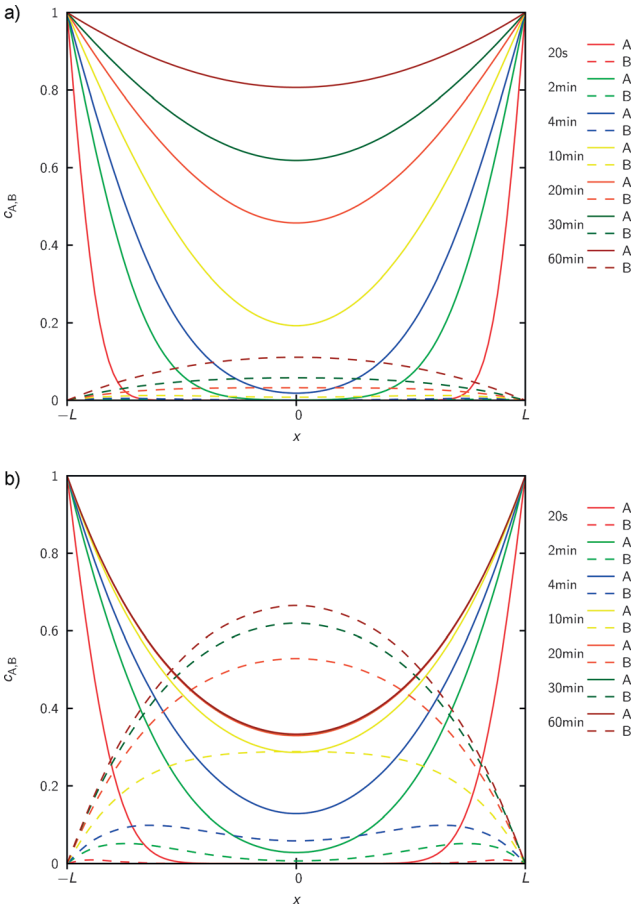

Figure 3. Complete presentation of the solution of the diffusion–reaction equation for hydrogenation of benzene to cyclohexane (a: 26 °C; b: 75 °C). Complementing Figure 2, the evolution of the concentration profiles (solid lines: benzene (A), dashed lines: cyclohexane (B)) is now shown for the whole of the distance, $0 \le x \le 2L = 1800$ μm, from one edge of the catalyst particle to the opposite edge.

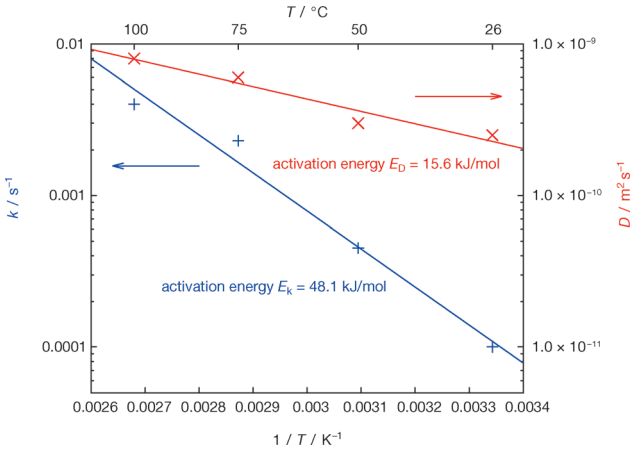

Figure 4. Arrhenius plots of the reaction rate constants and diffusivities. Analyzing the transient concentration profiles recorded at 26, 50, 75, and 100 °C (Figure 2; Supporting Information, Figure S7) yields the data shown in this figure. The straight lines result by fitting the Arrhenius law [Eqs. (5) and (6)] to these data, yielding the indicated activation energies.

(2)], justifying the simplifications inherent to the chosen approach.

Both these simplifications and unavoidable deficiencies in host structure do prevent total coincidence. The assumption of constant diffusivities for example is recognized as the origin of a systematic deviation of the benzene concentrations towards smaller values in comparison with the calculated ones, recorded for small concentrations at the beginning of our experiments. Under the conditions of single-component uptake, as given in the initial stage of our experiments, diffusivities increasing with concentration are well known to give rise to diffusion fronts steeper than for constant diffusivities.[25,29] Increase with increasing loading is a general feature of guest diffusivities in nanoporous materials during molecular uptake,[12] which in particular has been confirmed for the system under study.[21] Remaining differences may be referred to limited spatial resolution (Supporting Information)[30] and transport resistances acting along with the intrinsic diffusional resistance.[19]

Satisfactory agreement is also observed on comparing the absolute value of the diffusivity ($2.5 \pm 0.5 \times 10^{-10}\ m^2 s^{-1}$ at room temperature) with reported data[21] determined in both microscopic and macroscopic diffusion measurements with cyclohexane in the same host material (ca. 1 to $3 \times 10^{-10}\ m^2 s^{-1}$). Similarly, also the value of $48.1 \pm 4.9\ kJ\,mol^{-1}$ resulting from the temperature dependence of the reaction rate constant for the activation energy is within the range of values reported for hydrogenation reactions with nickel catalysts.[23,24,31]

In Figure 5, the results of our studies are presented within the context of conventional diffusivity–reactivity analyses by plotting the effectiveness factor η for irreversible reactions of first order:

$$\eta = \frac{\tanh \phi_L}{\phi_L} \tag{7}$$

as a function of the Thiele modulus ϕ_L

$$\phi_L = L\sqrt{k/D} \tag{8}$$

For these calculations we exploited the reactivities and diffusivities of Figure 4, which have been determined by analyzing the transient concentration profiles. Continuing the conventional way of presentation, the inset in Figure 5 also shows the reactant concentration profiles in the steady state. These profiles do clearly coincide with the solid lines in Figure 2 (and Supporting Information, Figure S7) attained in the limit of the largest observation times. The effectiveness factor is nothing else than the area below these profiles [resulting in Eq. (7), by integration over the stationary state profile; Supporting Information, Eq. (S33)]. We recognize the familiar pattern of effectiveness factors decreasing with increasing temperature corresponding with the faster increase of the reaction rate constants in comparison with the diffusivities (Figure 4).

Microimaging is able to record both the final concentration profiles and their evolution towards these patterns. The features becoming thus accessible by immediate observation include a remarkable difference in the rates by which the profiles of the reactant and product molecules approach their final shape. Whilst in the transient profiles shown in Figure 2b for 75 °C after 2 min the concentrations of the product molecules have emerged to not more than about 10 % of their value under steady-state conditions, the reactant concentrations have already attained close to three fourths of their steady-state values.

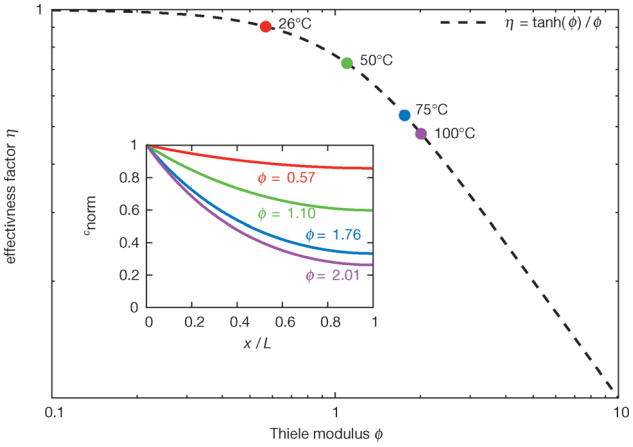

Figure 5. Effectiveness factor (data points, area below the steady-state reactant profiles in the insert) plotted as a function of the Thiele modulus and complemented by the complete representation of Equation (7).

Transient concentration profiles emerging in the interplay of diffusion and reaction in nanoporous materials, which so far have essentially been known from only textbook illustrations[11,12,25,32] have thus become accessible by direct microscopic observation, opening a novel route towards the determination of intrinsic diffusivities and reaction rate constants. These novel potentials include the determination of the effectiveness factor by mere inspection of the distribution of the reactant molecule within the catalyst particle.

Effectiveness factors were previously generally calculated by Equations (7) and (8) by determining the variation of the reactivity as a function of the variation of a suitably chosen parameter (mostly, the particle size), with the assumption that all other parameters (notably the diffusivities and intrinsic reaction rate constants) remain unaffected.[8–12] With the new procedure, there is no longer any need for such assumptions, which in general are hard to be confirmed with absolute reliability.[33] With the representation of the effectiveness factor (now directly accessible as illustrated by the inset) as a function of the Thiele modulus in Figure 5, the new way of analysis is, on the other hand, seen to be completely compatible with the well-established formalism of diffusion–reaction theory.

The system and reaction chosen allowed the demonstration of the feasibility and potentials of the novel principle of in situ measurement, even given the substantial limitations in both the temporal and spatial resolution as well as in the temperature range covered during the experiments. These limitations, however, are not of principle nature and shall be significantly released in the process of further experimental

and methodological development. With the realistic option of attaining resolutions in the range of seconds and a few micrometers and reaction temperatures up to several hundred centigrade, microimaging offers promising prospects for application in both fundamental research and catalyst development.

Keywords: glasses · heterogeneous catalysis · reaction kinetics · reaction mechanisms · supported catalysts

How to cite: *Angew. Chem. Int. Ed.* **2015**, *54*, 5060–5064
Angew. Chem. **2015**, *127*, 5148–5153

[1] a) H. Li, M. Eddaoudi, M. O'Keeffe, O. M. Yaghi, *Nature* **1999**, *402*, 276–279; b) S. Horike, S. Shimomura, S. Kitagawa, *Nat. Chem.* **2009**, *1*, 695–704.
[2] S. Mitchell, N.-L. Michels, K. Kunze, J. Perez-Ramirez, *Nat. Chem.* **2012**, *4*, 825–831.
[3] J. S. Seo, D. Whang, H. Lee, S. I. Jun, J. Oh, Y. J. Jeon, K. Kim, *Nature* **2000**, *404*, 982–986.
[4] a) J. Pérez-Ramírez, C. H. Christensen, K. Egeblad, C. H. Christensen, J. C. Groen, *Chem. Soc. Rev.* **2008**, *37*, 2530; b) J. Pérez-Ramírez, *Nat. Chem.* **2012**, *4*, 250–251; c) K. P. Möller, T. Bein, *Chem. Soc. Rev.* **2013**, *42*, 3689.
[5] G. Wang, M. O. Coppens, *Chem. Eng. Sci.* **2010**, *65*, 2344–2351.
[6] F. Jüttner, *Z. Phys. Chem.* **1909**, *65*, 595.
[7] a) E. W. Thiele, *Ing. Eng. Chem.* **1939**, *31*, 916–920; b) L. L. Hegedus, E. E. Petersen, *Catal. Rev.* **1974**, *9*, 245–266.
[8] L. Riekert, *Adv. Catal.* **1970**, *21*, 281–322.
[9] W. O. Haag, R. M. Lago, P. B. Weisz, *Faraday Discuss.* **1981**, *72*, 317–330.
[10] M. F. M. Post, J. van Amstel, H. W. Kouvenhoven in *Proc. Sixth Internat. Zeolite Conf.* (Eds.: D. Olson, A. Bisio), Butterworths, Guildford, **1984**.
[11] N. Y. Chen, T. F. Degnan, C. M. Smith, *Molecular Transport and Reaction in Zeolites*, VCH, New York, **1994**.
[12] J. Kärger, D. M. Ruthven, D. N. Theodorou, *Diffusion in Nanoporous Materials*, Wiley-VCH, Weinheim, **2012**.
[13] U. Hong, J. Kärger, B. Hunger, N. N. Feoktistova, S. P. Zhdanov, *J. Catal.* **1992**, *137*, 243–251.
[14] a) *Single Particle Tracking and Single Molecule Energy Transfer* (Eds.: C. Bräuchle, D. C. Lamb, J. Michaelis), Wiley-VCH, Weinheim, **2010**; b) B. M. Weckhuysen, *Angew. Chem. Int. Ed.* **2009**, *48*, 4910–4943; *Angew. Chem.* **2009**, *121*, 5008–5043.
[15] E. Stavitski, B. M. Weckhuysen, *Chem. Soc. Rev.* **2010**, *39*, 4615–4625.
[16] a) J. Kirstein, B. Platschek, C. Jung, R. Brown, T. Bein, C. Bräuchle, *Nat. Mater.* **2007**, *6*, 303–310; b) C. Jung, P. Schwaderer, M. Dethlefsen, R. Köhn, J. Michaelis, C. Bräuchle, *Nat. Nanotechnol.* **2011**, *6*, 87–92; c) G. De Cremer, M. B. J. Roeffaers, E. Bartholomeeusen, K. F. Lin, P. Dedecker, P. P. Pescarmona, P. A. Jacobs, D. E. de Vos, J. Hofkens, B. F. Sels, *Angew. Chem. Int. Ed.* **2010**, *49*, 908–911; *Angew. Chem.* **2010**, *122*, 920–923; d) I. L. C. Buurmans, B. M. Weckhuysen, *Nat. Chem.* **2012**, *4*, 873–886; e) L. Karwacki, M. H. F. Kox, D. A. M. de Winter, M. R. Drury, J. D. Meeldijk, E. Stavitski, W. Schmidt, M. Mertens, P. Cubillas, N. John, A. Chan, N. Kahn, S. R. Bare, M. Anderson, J. Kornatowski, B. M. Weckhuysen, *Nat. Mater.* **2009**, *8*, 959–965.
[17] F. Feil, S. Naumov, J. Michaelis, R. Valiullin, D. Enke, J. Kärger, C. Bräuchle, *Angew. Chem. Int. Ed.* **2012**, *51*, 1152–1155; *Angew. Chem.* **2012**, *124*, 1178–1181.
[18] a) J. Kärger, P. Kortunov, S. Vasenkov, L. Heinke, D. B. Shah, R. A. Rakoczy, Y. Traa, J. Weitkamp, *Angew. Chem. Int. Ed.* **2006**, *45*, 7846–7849; *Angew. Chem.* **2006**, *118*, 8010–8013; b) D. Tzoulaki, L. Heinke, W. Schmidt, U. Wilczok, J. Kärger, *Angew. Chem. Int. Ed.* **2008**, *47*, 3954–3957; *Angew. Chem.* **2008**, *120*, 4018–4021; c) D. Tzoulaki, L. Heinke, J. Li, H. Lim, D. Olson, J. Caro, R. Krishna, C. Chmelik, J. Kärger, *Angew. Chem. Int. Ed.* **2009**, *48*, 3525–3528; *Angew. Chem.* **2009**, *121*, 3577–3580; d) C. Chmelik, J. Kärger, *Chem. Soc. Rev.* **2010**, *39*, 4864–4884.
[19] J. Kärger, T. Binder, C. Chmelik, F. Hibbe, H. Krautscheid, R. Krishna, J. Weitkamp, *Nat. Mater.* **2014**, *13*, 333–343.
[20] a) F. Janowski, D. Enke in *Handbook of Porous Solids* (Eds.: F. Schüth, K. S. W. Sing, J. Weitkamp), Wiley-VCH, Weinheim, **2002**; b) D. Enke, F. Janowski, W. Schwieger, *Microporous Mesoporous Mater.* **2003**, *60*, 19–30.
[21] C. Chmelik, D. Enke, P. Galvosas, O. C. Gobin, A. Jentys, H. Jobic, J. Kärger, C. Krause, J. Kullmann, J. A. Lercher, S. Naumov, D. M. Ruthven, T. Titze, *ChemPhysChem* **2011**, *12*, 1130–1134.
[22] a) J. B. Butt, J. P. Irving, *Nature* **1966**, *212*, 1039–1040; b) M. Ziolek, *J. Catal.* **2001**, *199*, 162–170; c) M. Chettibi, A.-G. Boudjahem, M. Bettahar, *Transition Met. Chem.* **2011**, *36*, 163–169.
[23] P. Marecot, E. Paraiso, J. M. Dumas, J. Barbier, *Appl. Catal.* **1991**, *74*, 261–272.
[24] A. Lewandowska, S. Monteverdi, M. Bettahar, M. Ziolek, *J. Mol. Catal. A* **2002**, *188*, 85–95.
[25] J. Crank, *The Mathematics of Diffusion*, Clarendon Press, Oxford, **1975**.
[26] J. Kärger, S. Vasenkov, *Microporous Mesoporous Mater.* **2005**, *85*, 195–206.
[27] V. R. Choudhary, K. Mantri, *Langmuir* **2000**, *16*, 7031–7037.
[28] F. C. Meunier, D. Verboekend, J.-P. Gilson, J. C. Groen, J. Pérez-Ramírez, *Microporous Mesoporous Mater.* **2012**, *148*, 115–121.
[29] P. Kortunov, L. Heinke, S. Vasenkov, C. Chmelik, D. B. Shah, J. Kärger, R. A. Rakoczy, Y. Traa, J. Weitkamp, *J. Phys. Chem. B* **2006**, *110*, 23821–23828.
[30] C. Chmelik, H. Bux, J. Caro, L. Heinke, F. Hibbe, T. Titze, J. Kärger, *Phys. Rev. Lett.* **2010**, *104*, 085902.
[31] a) K. Yoon, *J. Catal.* **1983**, *82*, 457–468; b) B. Coughlan, M. A. Keane, *Zeolites* **1991**, *11*, 483–490.
[32] a) R. Aris, *The Mathematical Theory of Diffusion and Reaction in Permeable Catalysts*, Clarendon Press, Oxford, **1975**; b) H. S. Carslaw, J. C. Jaeger, *Conduction of Heat in Solids*, Oxford Science Publications, Oxford, **2004**.
[33] S. F. Garcia, P. B. Weisz, *J. Catal.* **1993**, *142*, 691–696.

Received: September 25, 2014
Revised: January 12, 2015
Published online: February 26, 2015

